On the Performance of Random Antenna Arrays for Direction of Arrival Estimation

Yaqoob, Muhammad Atif; Mannesson, Anders; Bernhardsson, Bo; Butt, Naveed; Tufvesson, Fredrik

Published in:
[Host publication title missing]

2014

On the Performance of Random Antenna Arrays for Direction of Arrival Estimation

Muhammad Atif Yaqoob*, Anders Mannesson†, Bo Bernhardsson†, Naveed R. Butt‡, Fredrik Tufvesson*
*Dept. of Electrical and Information Technology, Lund University, Lund, Sweden
†Dept. of Automatic Control, Lund University, Lund, Sweden
‡Centre For Mathematical Sciences, Lund University, Lund, Sweden
Email: Atif.Yaqoob@eit.lth.se

***Abstract*—A single antenna based virtual antenna array at the receiver can be used to find direction of different incoming radio signals impinging at the receiver. In this paper, we investigate the performance of random 3D virtual antenna arrays for DoA estimation. We have computed a Cramér-Rao Lower Bound (CRLB) for DoA estimation if the true antenna positions are not known, but these are estimated with an uncertainty. Position displacement is estimated with an extended Kalman filter (EKF) by using simulated data samples of acceleration and rotation rate which are corrupted by stochastic errors, such as, white Gaussian noise and bias drift. Furthermore, the effect of position estimation error on the DoA estimation performance is evaluated using the CRLB. The results show that the number of useful elements in the antenna array is limited, because the standard deviation of the position estimation error grows over time.**

***Index Terms*—Virtual Antenna Array, Direction of Arrival, Inertial Measurement Unit, Extended Kalman Filter, CRLB**

I. Introduction

In this paper, we investigate the performance of random 3D antenna arrays for direction of arrival (DoA) estimation. The array is formed using a single antenna element that is moved to different locations to form a so-called virtual antenna array. An inertial measurement unit (IMU) can be used to track the antenna positions as shown in [1], [2], where it has also been demonstrated that DoA estimation can be performed using such virtual antenna arrays. Since the antenna position is estimated from IMU measurements which are corrupted by noise, the antenna positions are known with an uncertainty associated with each antenna location. This work will describe that using such random antenna arrays, the number of useful antenna elements in the virtual antenna array is limited; because, the standard deviation of the antenna position estimation error grows over time. For a fixed antenna array geometry and signal to noise ratio (SNR), the variance of any unbiased DoA estimator can be lower bounded by a well known bound known as Cramér-Rao Lower Bound (CRLB). Different types of antenna arrays (linear arrays, 2D, and 3D arrays) have been suggested in the literature for different applications and their performance is evaluated with the help of CRLB [3]. Similarly, Cramér-Rao Bound can be used to have a lower bound on the performance of any unbiased estimator in the presence of antenna location uncertainties [4].

The contribution of this paper is to determine the performance limits of DoA estimation using low cost IMUs to make random antenna arrays. In the first part, we have simulated a six degrees of freedom (6DoF) navigation system performance using an IMU for random movements in 3D space. Acceleration and rotation rate data samples are simulated for a random 3D movement and the simulated data is then corrupted by stochastic errors, such as, white Gaussian noise and bias drift. Position displacement is estimated in the presence of these stochastic errors using an extended Kalman filter (EKF). In the second part, the effect of position errors on the DoA estimation performance is evaluated and the results are shown in the form of CRLB.

The paper is organized as follows. Firstly, a brief overview of inertial measurement unit (IMU) is given in section II. Section III describes the state space model to estimate the position displacement from the IMU measurements using the EKF. The Cramér-Rao lower bound on the DoA estimates is given in section IV. Results and discussion on the results is given in section V. Finally, conclusion is drawn in section VI.

II. Inertial Measurement Units

Inertial measurement units (IMUs) are often used as an integral part of navigation systems. An IMU today usually has orthogonal 3-axis accelerometers and 3-axis rate gyroscopes and it can provide inertial measurements of acceleration and rotation rate which are corrupted by noise. From the IMU measurements, by performing so-called double integration of the acceleration, also known as deadreckoning, the position displacement can be estimated. However, the IMU measurements should not directly be used for longer integration times as the different noise sources present in the measurements give rise to accumulated error upon integration. This requires that the position errors should be corrected periodically after a certain amount of integration time. Alternatively, the estimated position can be used for small integration times for which the uncertainty of the estimated position remains within a specified limit.

The noise/error sources in IMU measurements can be categorized into two main categories. The first category covers fixed or deterministic error sources and the second covers random or stochastic error sources. The first type of errors, such as cross-axis misalignment, scale factor, and non-linearity errors, can be determined by calibration before using the IMU for measurements, as suggested in [5]. Stochastic error sources

can be quantified by using a time domain analysis technique called Allan variance (AV) or a frequency domain analysis using power spectral decomposition (PSD) analysis [6], [7].

The Allan variance is a time domain technique originally developed by David W. Allan in 1966 to investigate the frequency stability of oscillators [8]. It has been successfully applied to model the different measurement errors in rate gyroscope and accelerometer measurements [6]. More details about Allan variance can be found in [9], [10]. In this work we will be using Allan variance analysis to quantify the stochastic errors present in the IMU measurements as shown in section III-C.

III. Extended Kalman Filter

The Kalman filter has remained a popular choice for navigation solutions since its inception in 1960 [11]. Over time, various extensions have been proposed to the standard Kalman filter for specific applications. In this work we are using an extended Kalman filter, as the process dynamics and the measurement relationship to the process that is to be estimated is nonlinear. A brief overview of Kalman filters is given in [12].

The state vector that is to be estimated using the extended Kalman filter is given as:

$$\mathbf{x} = [\mathbf{p}, \mathbf{v}, \mathbf{a}, \mathbf{a_b}, \mathbf{q}, \mathbf{w_b}]^T, \tag{1}$$

where $\mathbf{p}$=$[p_x, p_y, p_z]^T$ is the position displacement estimated in the world coordinate system. Similarly, $\mathbf{v} \in \mathbb{R}^3$ and $\mathbf{a} \in \mathbb{R}^3$ represent the three axis estimated velocity and acceleration in the world coordinate system. $\mathbf{q}$=$[q_0, q_1, q_2, q_3]^T$ is the unit quaternion that represents the orientation of the device w.r.t. the world coordinate system. Also, $\mathbf{a_b} \in \mathbb{R}^3$ and $\mathbf{w_b} \in \mathbb{R}^3$ are used to estimate the acceleration and rotation rate bias in the acceleration and rotation rate measurements, respectively.

A. State Update

The acceleration state in the world coordinate system is here modeled as a first order Gauss-Markov process. Let $\tilde{\mathbf{x}}$=$[\mathbf{p}, \mathbf{v}, \mathbf{a}]^T$, then the process dynamics for the position, velocity, and acceleration states defined in the world coordinate system are given by [13]:

$$\tilde{\mathbf{x}}_{k+1} = \tilde{\mathbf{F}}\tilde{\mathbf{x}}_k + \tilde{\mathbf{G}}\nu_{a,k}, \tag{2}$$

where $\tilde{\mathbf{F}}$ and $\tilde{\mathbf{G}}$ are defined as

$$\tilde{\mathbf{F}} = \begin{bmatrix} \mathbf{I}_3 & T_s\mathbf{I}_3 & (\alpha T_s - 1 + e^{-\alpha T_s})/\alpha^2\mathbf{I}_3 \\ \mathbf{0}_3 & \mathbf{I}_3 & (1 - e^{-\alpha T_s})/\alpha\mathbf{I}_3 \\ \mathbf{0}_3 & \mathbf{0}_3 & e^{-\alpha T_s}\mathbf{I}_3 \end{bmatrix}, \tag{3}$$

$$\tilde{\mathbf{G}} = \begin{bmatrix} (1 - \alpha T_s + \alpha^2\frac{T_s^2}{2} - e^{-\alpha T_s})/\alpha^3\mathbf{I}_3 \\ (\alpha T_s - 1 + e^{-\alpha T_s})/\alpha^2\mathbf{I}_3 \\ (1 - e^{-\alpha T_s})/\alpha\mathbf{I}_3 \end{bmatrix}, \tag{4}$$

where T_s is the sample time, $\mathbf{I}_3$ is a 3×3 identity matrix, $\mathbf{0}_3$ is a 3×3 matrix of all zeros, α=$1/\tau_a$ is the inverse of the time correlation of the acceleration, and ν_a is a zero mean white Gaussian noise sequence, which drives the acceleration process, with variance $\sigma^2_{\nu_a}$.

The state dynamics for the quaternion can be expressed as [14], [15]

$$\mathbf{q}_{k+1} = e^{\frac{T_s}{2}\mathbf{S_w}(\mathbf{w}_k^{true})}\mathbf{q}_k, \tag{5}$$

where $\mathbf{w}^{true}$ is the actual rotation rate.The measured rotation rate from the IMU is modeled as

$$\mathbf{w}^{meas} = \mathbf{w}^{true} + \mathbf{w_b} + \mathbf{e_w}, \tag{6}$$

where $\mathbf{w}^{meas} \in \mathbb{R}^3$ is the measured rotation rate that is the sum of actual rotation rate $\mathbf{w}^{true}$, bias in the sensor measurement $\mathbf{w}_b$, and measurement noise $\mathbf{e}_w$. The latter is modeled as zero mean white Gaussian noise with variance σ^2_w. Thus, the state dynamics for the quaternion is [14], [15]

$$\mathbf{q}_{k+1} = e^{\frac{T_s}{2}\mathbf{S_w}(\mathbf{w}_k^{meas})}\mathbf{q}_k - \frac{T_s}{2}\mathbf{S_q}(\mathbf{q}_k)\mathbf{w}_{b,k} - \frac{T_s}{2}\mathbf{S_q}(\mathbf{q}_k)\mathbf{e_{w,k}}, \tag{7}$$

The bias states for acceleration and rotation rates are modeled as first order Gauss-Markov processes. In discrete-time they can be modeled as

$$\mathbf{a}_{b,k+1} = a_{d,a}\mathbf{a}_{b,k} + b_{d,a}\nu_{\mathbf{a}_b,k}, \tag{8}$$

$$\mathbf{w}_{b,k+1} = a_{d,w}\mathbf{w}_{b,k} + b_{d,w}\nu_{\mathbf{w}_b,k}, \tag{9}$$

where $a_{d,a} = e^{-\frac{T_s}{\tau_{a_b}}}$ and $b_{d,a} = \int_0^{T_s} e^{-\frac{t}{\tau_{a_b}}}dt$. τ_{a_b} is the time constant for the acceleration bias drift process. Furthermore, $\nu_{\mathbf{a}_b}$ and $\nu_{\mathbf{w}_b}$ represent white noise processes with variances $\sigma^2_{\nu_{\mathbf{a}_b}}$ and $\sigma^2_{\nu_{\mathbf{w}_b}}$, respectively. These white noise processes drive the bias processes and their variances are given by

$$\sigma^2_{\nu_{\mathbf{a}_b}} = \frac{1 - a^2_{d,a}}{b^2_{d,a}}\sigma^2_{a_b}, \tag{10}$$

$$\sigma^2_{\nu_{\mathbf{w}_b}} = \frac{1 - a^2_{d,w}}{b^2_{d,w}}\sigma^2_{w_b}, \tag{11}$$

where $\sigma^2_{a_b}$ and $\sigma^2_{w_b}$ represents the variances of the accelerometer and rate gyroscope bias drift processes respectively.

B. Measurement Update

The acceleration state is related to the measurement through a nonlinear function as

$$\mathbf{a}_k^{meas} = \mathbf{R}_q(\mathbf{q}_k)(\mathbf{a}_k + \mathbf{g}) + \mathbf{a}_{b,k} + \mathbf{e}_{a,k}, \tag{12}$$

where $\mathbf{a}^{meas} \in \mathbb{R}^3$ is the measured acceleration in the body coordinate system, $\mathbf{R}_q(\mathbf{q})$ is the rotation matrix to transform the estimated acceleration that is in the world coordinate system to the body coordinate system, and $\mathbf{g}$ is acceleration in the world coordinate system due to gravity and is defined as $\mathbf{g}$=$[0, 0, 9.82]^T$. Also, the measured acceleration contains bias $\mathbf{a}_b$ as modeled in (8) and white Gaussian noise $\mathbf{e}_a$ with variance σ^2_a.

C. Simulation Parameters and Position Estimation

Using the Allan variance analysis, the stochastic error sources present in the IMU measurements are determined by recording static IMU data over a period of 8 hours. Fig. 1 shows the measured Allan deviation (AD) curve for x-axis accelerometer and for x-axis rate gyroscope, where Allan deviation is computed as the square root of the Allan variance.

For modeling the white noise and bias drift processes used in the EKF, it is assumed that errors on the y-axis and z-axis accelerometer are similar to the x-axis accelerometer. The same is assumed for the rate gyroscope measurements. Furthermore, it is also assumed that the deterministic errors are completely removed by calibration while the effect of stochastic errors is present on the position estimates.

From the Allan deviation plot of the accelerometer and rate gyroscope data, we can identify that white Gaussian noise and bias instability are the dominant error sources for short averaging times. The standard deviation for the accelerometer white noise is determined as σ_a=VRW/$\sqrt{T_s}$, where VRW is defined as the velocity random walk parameter and its numerical value can be obtained from the Allan deviation plot when the averaging time equals to 1. The slope of the Allan deviation plot equals to zero when the averaging time is 115 s. This sets the time constant for the bias drift as τ_{a_b}=115 s and the standard deviation for the process noise for bias drift is found as σ_{a_b}=AD(τ_{a_b})/0.664, where AD(τ_{a_b}) represents the numerical value of the Allan deviation plot when the averaging time equals to τ_{a_b}. Similarly, from the Allan deviation plot of the gyroscope data, we can obtain the standard deviation of the white noise process as well as the time constant for the bias drift process and the standard deviation for the white noise that drives the bias drift process. The sampling time (T_s) is set as 20 ms and the numerical values for the noise processes are obtained as: σ_a=4.15×10^{-3} m/s^2, σ_w=0.115 °/s, σ_{a_b}=2.85×10^{-4} m/s^2, and σ_{w_b}=7.5×10^{-3} °/s. Also, τ_{w_b} is estimated as 115 s.

To simulate a random antenna array in 3D, acceleration as well as rotation rate data samples are generated using the Singer model [13]. This model is a maneuver model often used to model target maneuvering. As the antenna is moved by holding it in a hand to follow any random trajectory, the Singer model can be used to model such a movement. The Singer model states that the acceleration or rotation rate follows a first order Gauss-Markov process. In discrete time, it can be described as $\mathbf{a}_{k+1}$=$a_d\mathbf{a}_k + b_d\nu_{\mathbf{a}_k}$, where a_d=$e^{-\frac{T_s}{\tau_a}}$ and b_d=$\int_0^{T_s} e^{-\frac{t}{\tau_a}}\,dt$. τ_a is the maneuver time constant for the accelerometer data. Also, $\nu_{\mathbf{a_k}}$ is a white noise sequence with variance $\sigma^2_{\nu_\mathbf{a}}$=$\frac{1-a_d^2}{b_d^2}\sigma^2_{acc}$, where σ^2_{acc}=$\frac{a^2_{\max}}{3}(1+4P_{\max}-P_0)$. $a_{\max}$ is the maximum acceleration/deceleration during the maneuver, whereas, $P_{\max}$ and P_0 models the probability of having maximum acceleration/deceleration and zero acceleration during the maneuver [13]. We have used τ_a=2.5 s, $a_{\max}$=1 m/s^2, P_0=0.99, and $P_{\max}$=0.01 for the acceleration data samples. For rotation rate data, the parameter for maximum rotation rate is set to $w_{\max}$=600 °/s, while the other parameters are the same as for the acceleration. Acceleration and rotation rate data samples are then added with noise which is simulated using the values obtained from Allan deviation plots as described above. Position displacement is then estimated along-with the other states mentioned in (1) using an EKF. Fig. 2 shows a typical plot for the position estimation error standard deviation that is estimated using the EKF. From Fig. 2, it can be noted that the standard deviation in the estimated antenna position, as expected, grows over time. Also, the uncertainty in the x- and y-axes is similar while the z-axis has lower uncertainty as compared to the x- and y-axes. For any small tilt error (ζ) in the device orientation, the residual acceleration due to gravity on x- and y-axis would be approximated by $\sin(\zeta)$ and along z-axis it would be $\cos(\zeta)$. Using small angle approximation, $\sin(\zeta) = \zeta$ and $\cos(\zeta) = 1$. Therefore, as the gravity acceleration is along the z-axis, the residual acceleration after removing acceleration due to gravity would be larger along the x- and y-axes as compared to the z-axis.

IV. Cramér Rao Lower Bound for DoA Estimation

In this section we will determine the CRLB for an antenna array where the antenna elements are defined in 3D space using Cartesian coordinates. Two different scenarios are considered to compute the CRLB. In section IV-A, the CRLB is computed when true antenna positions are known and section

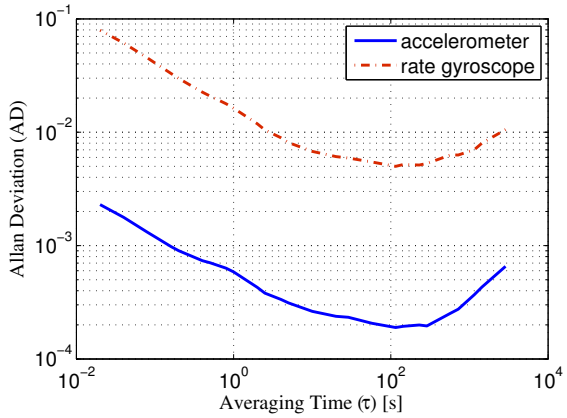

Fig. 1. Measured Allan deviation (AD) plot for x-axis accelerometer and x-axis rate gyroscope data. AD is measured in m/s^2 for accelerometer data and $^\circ/s$ for rate gyroscope.

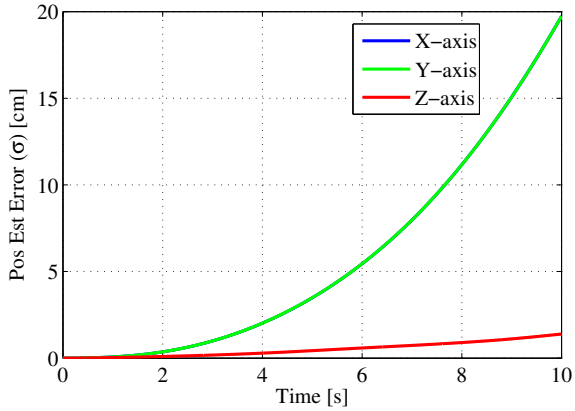

Fig. 2. Position estimation error standard deviation from the EKF, x- and y-axes have similar position estimation error std. deviation vs time while z-axis has smaller std. deviation values as compared to the x- and y-axes.

IV-A provides the derivation of the CRLB when the antenna positions are estimated with an uncertainty associated with each antenna position.

A. CRLB with Known Antenna Positions

An incoming radio signal received from a narrowband far-field source at an antenna array comprising of N isotropic antenna elements can be defined as:

$$\mathbf{y_r} = \alpha_r \mathbf{s}(\phi, \theta) + \mathbf{e_r}, \tag{13}$$

where $\mathbf{y_r} \in \mathbb{C}^{N\times 1}$ is the received signal vector, $\alpha_r{=}ae^{jb}$ is the complex amplitude of the received radio signal (where a is the amplitude and b is the phase), $\mathbf{e}_r \in \mathbb{C}^{N\times 1}$ is the complex Gaussian white noise having covariance matrix $\mathbf{R_r}{=}\sigma_r^2\mathbf{I}$, and $\mathbf{s}(\phi,\theta)$ is the array response vector and is given by:

$$\mathbf{s}(\phi,\theta) = e^{jk(\mathbf{x}\cos(\phi)\sin(\theta)+\mathbf{y}\sin(\phi)\sin(\theta)+\mathbf{z}\cos(\theta))}, \tag{14}$$

where $\mathbf{x}$, $\mathbf{y}$, and $\mathbf{z}$ are position coordinate vectors defining the antenna elements in 3D space. Also, ϕ is the DoA of the incoming radio signal in the azimuth whereas θ is the DoA in the elevation, and $k{=}2\frac{\pi}{\lambda}$.

The probability density function of the received signal can be expressed as [3]

$$p(\mathbf{y_r};\Theta) = \frac{1}{\pi^N det(\mathbf{R_r})} e^{-(\mathbf{y_r}-\alpha_r\mathbf{s}(\phi,\theta))^H \mathbf{R_r^{-1}} (\mathbf{y_r}-\alpha_r\mathbf{s}(\phi,\theta))}, \tag{15}$$

where $\Theta{=}[a,b,\phi,\theta]$ are the unknown parameters. The Fisher information matrix $\mathbf{I}(\Theta)$ can then be found as:

$$\mathbf{I}(\Theta)_{ij} = -E_{\mathbf{y_r}}[\frac{\partial^2 \ln p(\mathbf{y_r};\Theta)}{\partial\Theta_i\partial\Theta_j}], \tag{16}$$

where $\mathbf{I}(\Theta)_{ij}$ represents the $(i,j)^{th}$ element of the $4{\times}4$ Fisher information matrix and $i,j \in [a,b,\phi,\theta]$. The expressions for the different entries in the Fisher information matrix $\mathbf{I}(\Theta)$ are determined as shown in (17)-(23):

$$-E_{\mathbf{y_r}}[\frac{\partial^2 \ln p(\mathbf{y_r};\Theta)}{\partial a^2}] = \frac{2N}{\sigma_r^2}, \tag{17}$$

$$-E_{\mathbf{y_r}}[\frac{\partial^2 \ln p(\mathbf{y_r};\Theta)}{\partial b^2}] = \frac{2Na^2}{\sigma_r^2}, \tag{18}$$

$$-E_{\mathbf{y_r}}[\frac{\partial^2 \ln p(\mathbf{y_r};\Theta)}{\partial \phi^2}] = \frac{2a^2}{\sigma_r^2}k^2\sum_{n=1}^{N} A_n^2, \tag{19}$$

$$-E_{\mathbf{y_r}}[\frac{\partial^2 \ln p(\mathbf{y_r};\Theta)}{\partial \theta^2}] = \frac{2a^2}{\sigma_r^2}k^2\sum_{n=1}^{N} B_n^2, \tag{20}$$

$$-E_{\mathbf{y_r}}[\frac{\partial^2 \ln p(\mathbf{y_r};\Theta)}{\partial b\partial \phi}] = -\frac{2a^2}{\sigma_r^2}k\sum_{n=1}^{N} A_n, \tag{21}$$

$$-E_{\mathbf{y_r}}[\frac{\partial^2 \ln p(\mathbf{y_r};\Theta)}{\partial b\partial \theta}] = \frac{2a^2}{\sigma_r^2}k\sum_{n=1}^{N} B_n, \tag{22}$$

$$-E_{\mathbf{y_r}}[\frac{\partial^2 \ln p(\mathbf{y_r};\Theta)}{\partial \phi\partial \theta}] = -\frac{2a^2}{\sigma_r^2}k^2\sum_{n=1}^{N} A_nB_n, \tag{23}$$

where

$$A_n = (x_n\sin(\phi) - y_n\cos(\phi))\sin(\theta), \tag{24}$$

$$B_n = (x_n\cos(\phi) + y_n\sin(\phi))\cos(\theta) - z_n\sin(\theta). \tag{25}$$

The remaining elements of the Fisher information matrix are computed to be zero. The CRLB can then be obtained as the inverse of the Fisher information matrix.

B. CRLB with Estimated Antenna Positions

If the true antenna positions are not known but we have an estimate of the antenna position, e.g., for the n^{th} antenna element where $n{=}1,2,\cdots,N$, let's assume (x_n,y_n,z_n) corresponds to the true antenna position represented in the 3D space and $\Delta x_n, \Delta y_n, \Delta z_n$ are the position errors along the x-, y-, and z-axis respectively. Then, the estimated position coordinates can be represented as $(x_n{+}\Delta x_n, y_n{+}\Delta y_n, z_n{+}\Delta z_n)$. Furthermore, the position errors for the n^{th} antenna element are modeled as independent zero mean white Gaussian noise processes with variances $\sigma_{x_n}^2$, $\sigma_{y_n}^2$, and $\sigma_{z_n}^2$, for the x-, y-, and z-axis, respectively. In this case, the unknown parameters would become $4+3N$, and are shown in (26)

$$\Theta = [a,b,\phi,\theta, \Delta x_1,\Delta y_1,\Delta z_1,\Delta x_2,\Delta y_2,\Delta z_2,\cdots,\Delta x_N,\Delta y_N,\Delta z_N] \tag{26}$$

Therefore, we will have deterministic unknown parameters as well as random unknown parameters. With random unknown parameters, the Fisher information matrix is defined as [4]

$$\mathbf{I}(\Theta)_{ij} = \mathbf{I}_1(\Theta)_{ij} + \mathbf{I}_2(\Theta)_{ij}, \tag{27}$$

where $i,j \in \Theta$, set of unknown parameters as shown in (26), and the two different elements of the Fisher information matrix are expressed as

$$\mathbf{I}_1(\Theta)_{ij} = -E_{\mathbf{y_r},\Theta}[\frac{\partial^2 \ln p(\mathbf{y_r};\Theta)}{\partial\Theta_i\partial\Theta_j}] \tag{28}$$

$$\mathbf{I}_2(\Theta)_{ij} = -E_{\Theta}[\frac{\partial^2 \ln p(\Theta)}{\partial\Theta_i\partial\Theta_j}]. \tag{29}$$

The elements of the Fisher information matrix in $\mathbf{I}_1(\Theta)$ can be found as shown in (30)-(51), where $l,m{=}1,2,3,\cdots,N$. Also, $A_1{=}\cos(\phi)\sin(\theta)$, $A_2{=}\sin(\phi)\sin(\theta)$, and $A_3{=}\cos(\theta)$.

$$-E_{\mathbf{y_r},\Theta}[\frac{\partial^2 \ln p(\mathbf{y_r};\Theta)}{\partial a^2}] = \frac{2N}{\sigma_r^2} \tag{30}$$

$$-E_{\mathbf{y_r},\Theta}[\frac{\partial^2 \ln p(\mathbf{y_r};\Theta)}{\partial b^2}] = \frac{2Na^2}{\sigma_r^2} \tag{31}$$

$$-E_{\mathbf{y_r},\Theta}[\frac{\partial^2 \ln p(\mathbf{y_r};\Theta)}{\partial b\partial \phi}] = -\frac{2a^2}{\sigma_r^2}k\sum_{n=1}^{N} A_n \tag{34}$$

$$-E_{\mathbf{y_r},\Theta}[\frac{\partial^2 \ln p(\mathbf{y_r};\Theta)}{\partial b\partial \theta}] = \frac{2a^2}{\sigma_r^2}k\sum_{n=1}^{N} B_n \tag{35}$$

$$-E_{\mathbf{y_r},\Theta}[\frac{\partial^2 \ln p(\mathbf{y_r};\Theta)}{\partial \Delta x_l\partial \Delta x_m}] = \begin{cases} \frac{2a^2}{\sigma_r^2}k^2A_1^2 & \text{if } l=m, \\ 0 & \text{if } l\neq m. \end{cases} \tag{37}$$

$$-E_{\mathbf{y_r},\Theta}[\frac{\partial^2 \ln p(\mathbf{y_r};\Theta)}{\partial \phi^2}] = \frac{2a^2}{\sigma_r^2}k^2\sum_{n=1}^{N}[(x_n^2+\sigma_{x_n}^2)\sin^2(\phi)+(y_n^2+\sigma_{y_n}^2)\cos^2(\phi)-2x_ny_n\sin(\phi)\cos(\phi)]\sin^2(\theta) \quad (32)$$

$$-E_{\mathbf{y_r},\Theta}[\frac{\partial^2 \ln p(\mathbf{y_r};\Theta)}{\partial \theta^2}] = \frac{2a^2}{\sigma_r^2}k^2\sum_{n=1}^{N}[((x_n^2+\sigma_{x_n}^2)\cos^2(\phi)+(y_n^2+\sigma_{y_n}^2)\sin^2(\phi))\cos^2(\theta)+(z_n^2+\sigma_{z_n}^2)\sin^2(\theta) +2(x_ny_n\cos(\phi)\sin(\phi)\cos(\theta)-y_nz_n\sin(\phi)\sin(\theta)-x_nz_n\cos(\phi)\sin(\theta))\cos(\theta)] \quad (33)$$

$$-E_{\mathbf{y_r},\Theta}[\frac{\partial^2 \ln p(\mathbf{y_r};\Theta)}{\partial \phi \partial \theta}] = -\frac{2a^2}{\sigma_r^2}k^2\sum_{n=1}^{N}[((x_n^2+\sigma_{x_n}^2)-(y_n^2+\sigma_{y_n}^2))\sin(\phi)\cos(\phi)\sin(\theta)\cos(\theta) +x_ny_n(\sin^2(\phi)-\cos^2(\phi))\sin(\theta)\cos(\theta)-z_n(x_n\sin(\phi)-y_n\cos(\phi))\sin^2(\theta)] \quad (36)$$

$$-E_{\mathbf{y_r},\Theta}[\frac{\partial^2 \ln p(\mathbf{y_r};\Theta)}{\partial \Delta y_l \partial \Delta y_m}] = \begin{cases} \frac{2a^2}{\sigma_r^2}k^2A_2^2 & \text{if } l=m, \\ 0 & \text{if } l\neq m. \end{cases} \quad (38)$$

$$-E_{\mathbf{y_r},\Theta}[\frac{\partial^2 \ln p(\mathbf{y_r};\Theta)}{\partial \Delta z_l \partial \Delta z_m}] = \begin{cases} \frac{2a^2}{\sigma_r^2}k^2A_3^2 & \text{if } l=m, \\ 0 & \text{if } l\neq m. \end{cases} \quad (39)$$

$$-E_{\mathbf{y_r},\Theta}[\frac{\partial^2 \ln p(\mathbf{y_r};\Theta)}{\partial \Delta x_l \partial \Delta y_m}] = \begin{cases} \frac{2a^2}{\sigma_r^2}k^2A_1A_2 & \text{if } l=m, \\ 0 & \text{if } l\neq m. \end{cases} \quad (40)$$

$$-E_{\mathbf{y_r},\Theta}[\frac{\partial^2 \ln p(\mathbf{y_r};\Theta)}{\partial \Delta x_l \partial \Delta z_m}] = \begin{cases} \frac{2a^2}{\sigma_r^2}k^2A_1A_3 & \text{if } l=m, \\ 0 & \text{if } l\neq m. \end{cases} \quad (41)$$

$$-E_{\mathbf{y_r},\Theta}[\frac{\partial^2 \ln p(\mathbf{y_r};\Theta)}{\partial \Delta y_l \partial \Delta z_m}] = \begin{cases} \frac{2a^2}{\sigma_r^2}k^2A_2A_3 & \text{if } l=m, \\ 0 & \text{if } l\neq m. \end{cases} \quad (42)$$

$$-E_{\mathbf{y_r},\Theta}[\frac{\partial^2 \ln p(\mathbf{y_r};\Theta)}{\partial b \partial \Delta x_n}] = \frac{2a^2}{\sigma_r^2}kA_1 \quad (43)$$

$$-E_{\mathbf{y_r},\Theta}[\frac{\partial^2 \ln p(\mathbf{y_r};\Theta)}{\partial b \partial \Delta y_n}] = \frac{2a^2}{\sigma_r^2}kA_2 \quad (44)$$

$$-E_{\mathbf{y_r},\Theta}[\frac{\partial^2 \ln p(\mathbf{y_r};\Theta)}{\partial b \partial \Delta z_n}] = \frac{2a^2}{\sigma_r^2}kA_3 \quad (45)$$

$$-E_{\mathbf{y_r},\Theta}[\frac{\partial^2 \ln p(\mathbf{y_r};\Theta)}{\partial \phi \partial \Delta x_n}] = -\frac{2a^2}{\sigma_r^2}k^2A_1A_n \quad (46)$$

$$-E_{\mathbf{y_r},\Theta}[\frac{\partial^2 \ln p(\mathbf{y_r};\Theta)}{\partial \phi \partial \Delta y_n}] = -\frac{2a^2}{\sigma_r^2}k^2A_2A_n \quad (47)$$

$$-E_{\mathbf{y_r},\Theta}[\frac{\partial^2 \ln p(\mathbf{y_r};\Theta)}{\partial \phi \partial \Delta z_n}] = -\frac{2a^2}{\sigma_r^2}k^2A_3A_n \quad (48)$$

$$-E_{\mathbf{y_r},\Theta}[\frac{\partial^2 \ln p(\mathbf{y_r};\Theta)}{\partial \theta \partial \Delta x_n}] = \frac{2a^2}{\sigma_r^2}k^2A_1B_n \quad (49)$$

$$-E_{\mathbf{y_r},\Theta}[\frac{\partial^2 \ln p(\mathbf{y_r};\Theta)}{\partial \theta \partial \Delta y_n}] = \frac{2a^2}{\sigma_r^2}k^2A_2B_n \quad (50)$$

$$-E_{\mathbf{y_r},\Theta}[\frac{\partial^2 \ln p(\mathbf{y_r};\Theta)}{\partial \theta \partial \Delta z_n}] = \frac{2a^2}{\sigma_r^2}k^2A_3B_n \quad (51)$$

The remaining elements of $\mathbf{I}_1(\Theta)$ are found to be zero. The other part of the Fisher information matrix, i.e., $\mathbf{I}_2(\Theta)$ can be found as shown in (52), where the position errors are modeled as independent zero mean white Gaussian noise processes at each antenna location and also for the x-, y-, and z-axes as well.

$$\mathbf{I}_2(\Theta) = \begin{bmatrix} 0_{4\times4} & 0_{4\times3N} \\ 0_{3N\times4} & \Sigma^{-1}_{3N\times3N} \end{bmatrix} \quad (52)$$

where $0_{4\times4}$ is a 4×4 matrix of all zeros for the deterministic unknown parameters and $\Sigma_{3N\times3N}$ is a diagonal matrix representing the variance of the position errors along its diagonal and is defined as $\Sigma_{3N\times3N}=diag(\sigma_{x_1}^2,\sigma_{y_1}^2,\sigma_{z_1}^2,\cdots,\sigma_{x_N}^2,\sigma_{y_N}^2,\sigma_{z_N}^2)$, where the first three diagonal elements represent the position error variance of the first antenna element and the last three elements define the position error variance of the last antenna element, for x-, y-, and z-axis respectively.

V. Results and Discussion

In this section, using the position estimation error standard deviation values as shown in Fig. 2, we have computed two CRLB plots for the two cases mentioned in section IV, i.e., when the antenna positions are known and when the antenna

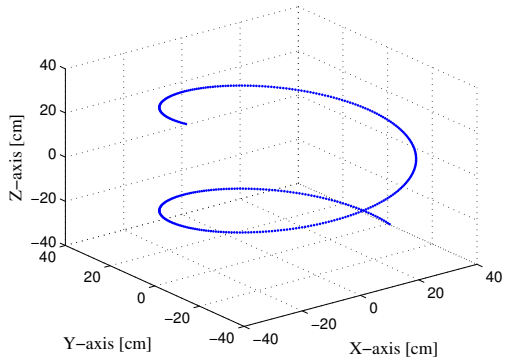

Fig. 3. An antenna array in 3D where different points in the plot represent the antenna positions. The array is used to analyze the performance of DoA estimation with known and estimated antenna positions through CRLB plots.

positions are estimated with an uncertainty. Radio signal centre frequency is set as f_c=2.4 GHz, and signal to noise ratio at the receiving antenna elements is assumed to be 0 dB. An antenna array geometry as shown in Fig. 3 is defined in 3D where the origin is at the center of gravity of the array. The CRLB plots are then obtained and are shown in Fig. 4 for a given DoA$(30°, 30°)$. In the CRLB plots, x-axis represents the number of antenna elements that span the antenna array for different movement times. The sampling time is used as 20 ms to simulate the IMU as well as radio samples. The given sampling rate provides 50 antenna positions after 1 second of the movement time and so on. In order to analyze the effect of growing standard deviation of the position estimation error onto the DoA estimation accuracy, different movement times are used such that each movement covers the same trajectory but with different time by changing the speed of the movement. Thus, the number of antenna elements that span the whole trajectory are varied but the array shape is kept the same. The CRLB values are then calculated corresponding to different movement times. From the plot when antenna positions are known it can be seen that as time increases, i.e., more antenna elements are used to represent the antenna array, then the CRLB decreases because with the increase of antenna elements the SNR is improved and the array resolution is enhanced as well. Thus, the DoA estimation could be performed with better accuracy. However, if the antenna positions are not known and are estimated with an uncertainty whose standard deviation is also growing, then, in this case the CRLB first decreases with increasing antennas. But, as time goes more than 3 second, we can observe that the CRLB plot starts to deviate from the plot where the antenna positions are known and the difference between the two CRLB plots grows over time. The growing standard deviation of the antenna position estimation error plays a significant role in limiting the performance of the DoA estimation as we observe for the case when antenna positions are known. The standard deviation of the position estimation error is relatively small in the beginning or for short integration times, but the standard deviation grows over time and we can observe that the gap between the two CRLB plots also grows over time as well. Therefore, it is found that an optimal time limit should be determined in order to make the virtual antenna array where the antenna positions are obtained with relatively small position estimation errors. For the given standard deviation of the antenna position estimation errors, as shown in Fig. 2, the optimal time in terms of DoA estimation performance is found to be approximately 3-4 seconds, and after this time limit we can see significant difference of the DoA estimation accuracy between the two CRLB plots. Similar results can be seen when the SNR is set as 10 dB.

As described above, similar analysis can be performed to estimate the performance of any random 3D antenna array if the antenna positions are known with an uncertainty. Fig. 5 shows an example of a random 3D antenna array and in Fig. 6 CRLB plots are shown. The two examples of 3D antenna arrays illustrate the usefulness of the given framework to compute the CRLB with known and estimated antenna positions. More detailed analysis of the results in terms of DoA estimation accuracy w.r.t. the different array shapes will be treated in our future work.

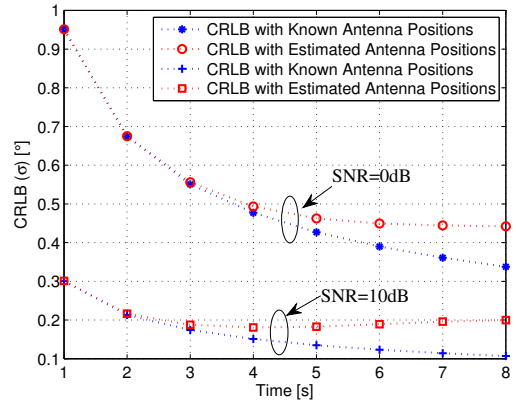

Fig. 4. CRLB for estimating (ϕ) for a given DoA(30°, 30°) using the antenna array shown in Fig. 3. 1 s corresponds to 50 antenna elements array obtained from IMU data samples where the IMU is sampled at a rate of 20 ms.

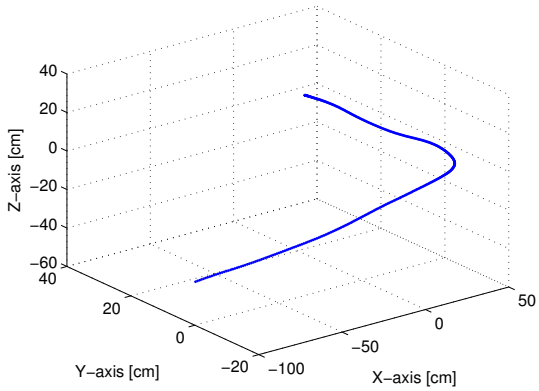

Fig. 5. Example of a random 3D antenna array.

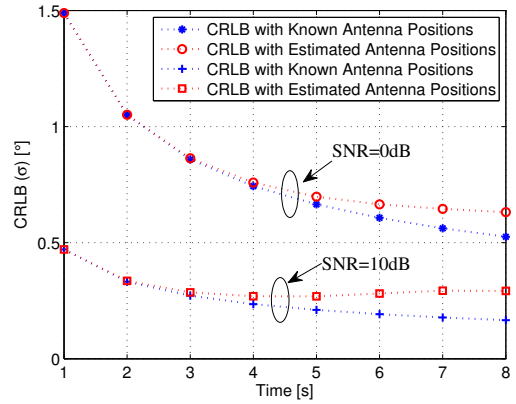

Fig. 6. CRLB for estimating (ϕ) for a given DoA(30°, 30°) using the antenna array shown in Fig. 5.

VI. Conclusion

In this paper, we have shown that the performance of virtual antenna arrays using inertial measurement units is limited by the growing standard deviation of the antenna position estimation errors. The effect of stochastic error sources, such as, white Gaussian noise and bias drift in the IMU measurements is investigated using EKF, which shows that the standard deviation of the position estimation error grows over time. Furthermore, we have computed Cramér-Rao lower bound (CRLB) if the antenna positions are known and if the antenna positions are estimated with an uncertainty. Using these two CRLB values, it has been shown that after a specific integration time, the increase in the standard deviation of the position estimation error plays a significant role and the increase in the number of antenna elements does not provide significant improvement in the performance of DoA estimation. For a low cost MEMS based IMU making a typical 3D movement, the optimal integration/movement time in terms of DoA estimation performance has been found to be approximately 3-4 seconds.

Acknowledgment

This work is supported by the Excellence Center at Linköping-Lund in Information Technology (www.elliit.liu.se) and by the Lund Center for Control of Complex Engineering Systems (www.lccc.lth.se) as well as the Swedish Research Council. The support is gratefully acknowledged.

References

[1] M. Yaqoob, F. Tufvesson, A. Mannesson, and B. Bernhardsson, "Direction of arrival estimation with arbitrary virtual antenna arrays using low cost inertial measurement units," in *Communications Workshops (ICC), 2013 IEEE International Conference on*, 2013, pp. 79–83.

[2] A. Broumandan, T. Lin, A. Moghaddam, D. Lu, J. Nielsen, and G. Lachapelle, "Direction of arrival estimation of GNSS signals based on synthetic antenna array," in *ION 2007, Fort Worth, TX*, 2007.

[3] X. Yang, T. Long, and T. Sarkar, "Effect of geometry of planar antenna arrays on Cramer-Rao Bounds for DOA estimation," in *Signal Processing (ICSP), 2010 IEEE 10th International Conference on*, 2010, pp. 389–392.

[4] J. Zhu and H. Wang, "Effects of sensor position and pattern perturbations on CRLB for direction finding of multiple narrow-band sources," in *Spectrum Estimation and Modeling, 1988., Fourth Annual ASSP Workshop on*, 1988, pp. 98–102.

[5] I. Skog and P. Hndel, "Calibration of a MEMS inertial measurement unit," in *Proc. XVII IMEKO WORLD CONGRESS, (Rio de Janeiro)*, 2006.

[6] N. El-Sheimy, H. Hou, and X. Niu, "Analysis and modeling of inertial sensors using Allan variance," *Instrumentation and Measurement, IEEE Transactions on*, vol. 57, no. 1, pp. 140–149, 2008.

[7] P. Petkov and T. Slavov, "Stochastic modeling of MEMS inertial sensors," *Cybernetics and information technologies*, vol. 10, no. 2, pp. 31–40, 2010.

[8] D. Allan, "Statistics of atomic frequency standards," *Proceedings of the IEEE*, vol. 54, no. 2, pp. 221–230, 1966.

[9] "IEEE standard specification format guide and test procedure for single-axis interferometric fiber optic gyros," *IEEE Std 952-1997*, 1998.

[10] M. M. Tehrani, "Ring Laser gyro data analysis with cluster sampling technique," *Proc. SPIE*, vol. 412, pp. 207–220, 1983.

[11] R. E. Kalman, "A new approach to linear filtering and prediction problems," *Transactions of the ASME - Journal of Basic Engineering*, no. 82, pp. 35–45, 1960.

[12] W. Greg and G. Bishop, "An introduction to the Kalman filter," Department of computer science, University of north Carolina at chapel hill, Tech. Rep. TR 95-041, 2006.

[13] X. Li and V. Jilkov, "Survey of maneuvering target tracking. Part I: Dynamic models," *Aerospace and Electronic Systems, IEEE Transactions on*, vol. 39, no. 4, pp. 1333–1364, 2003.

[14] E. J. Lefferts, F. L. Markley, and M. D. Shuster, "Kalman filtering for spacecraft attitude estimation," *Journal of Guidance, Control, and Dynamics*, vol. 5, no. 5, pp. 417–429, 1982.

[15] W.-T. Ang, P. Khosla, and C. Riviere, "Kalman filtering for real-time orientation tracking of handheld microsurgical instrument," in *Proceedings of the IEEE International Conference on Intelligent Robots and Systems*, vol. 3, 2004, pp. 2574–2580.